Tumor-Targeted Hyaluronan Nanoliposomes Increase the Antitumor Activity of Liposomal Doxorubicin in Syngeneic and Human Xenograft Mouse Tumor Models

Dan Peer and Rimona Margalit

Department of Biochemistry, The George S. Wise, Life Science Faculty, Tel-Aviv University, Tel Aviv, Israel

Abstract

Naturally occurring high-M_r hyaluronan, bound to the surface of nanoliposomes (denoted targeted hyaluronan liposomes, or tHA-LIP), is a candidate for active targeting to tumors, many of which overexpress the hyaluronan receptors CD44 and RHAMM. The surface-bound hyaluronan also provides a hydrophilic coat that, similar to polyethylene glycol, may promote long-term circulation. We recently reported the successful targeting of mitomycin C, mediated by tHA-LIP, in tumor-bearing syngeneic mice. Hypothesizing that this targeting is carrier-specific, rather than drug-specific, we report here studies with doxorubicin (DXR)–loaded tHA-LIP, in syngeneic and human xenograft models. Saline, free DXR, DXR-loaded nontargeted liposomes (nt-LIP), and Doxil served as controls. The tHA-LIP were long-circulating, more than all controls, in healthy and tumor-bearing (C57BL/6/B16F10.9; BALB/c/C-26) mice. Mediated by tHA-LIP, DXR accumulation in tumor-bearing lungs was 30-, 6.7-, and 3.5-fold higher than free DXR, nt-LIP, and Doxil, respectively. Key indicators of therapeutic responses—tumor progression, metastatic burden, and survival—were superior ($P < .001$) in animals receiving DXR-loaded tHA-LIP compared with controls, in tumor-bearing syngeneic mice (BDF$_1$/P388/ADR ascites, C57BL/6/B16F10.9 lung metastasis, and BALB/c/C-26 solid tumors), and in nude mice bearing PANC-1 solid tumors. In conclusion, tHA-LIP, performing as tumor-targeted carriers, have the potential to join the arsenal of carrier-formulated anticancer drugs.

Neoplasia (2004) **6**, 343–353

Introduction

Effective tumor chemotherapy requires targeting the anticancer drug to its molecular sites of action. Random, nontargeted distribution of the drug within the living system reduces therapeutic efficacy and, at the same time, increases the risks of undesirable side effects and toxicity [1–4]. Because few anticancer drugs are capable of self-targeting [5,6], a major approach to achieve this goal is to entrap the drug in a particulate carrier, delegating the tumor-targeting responsibility to the carrier.

Targeting systemically administered particulate carriers to tumors localized outside the reticuloendothelial system (RES), namely "active targeting" [1–4,7–14], requires the combination of long-term circulation, particle extravasation to the tumor, and high affinity to tumor-localized recognition sites. Tumor physiology both lends a hand and poses obstacles to targeting. Normally, particulate carriers are unable to extravasate from the circulation. However, the rather leaky vascular system reported for many tumors [9,10] allows particulate carriers, such as liposomes, some measure of extravasation from the circulation into the tumor. Yet, the RES usually acts to fast-remove particles from the circulation, which prevents them from reaping the benefits of the leaky tumor circulation. A breakthrough in countering this fast removal was achieved when it was found that nanosized particles, and more so a combination of small size and hydrophilic surface, delay RES uptake [2,4,12,13,15–17].

Yet, carrier-mediated drug targeting to tumors, *in vivo*, is still an elusive goal. Neither the intrinsic carrier components nor the hydrophilic coat endows the particles with high affinity to tumor-localized recognition sites. It usually requires positioning an appropriate agent on the particle's surface and such agents, effective *in vivo*, are hard to come by. Feasibility of efforts that are underway, using two agents (one for long circulation, and the other for tumor binding), will depend on whether the risks of mutual interferences can be satisfactorily resolved [18,19].

We hypothesized that our bioadhesive nanoliposomes [7,8,16,20–24], with the naturally occurring high M_r ($\sim 10^6$ Da)

hyaluronan anchored covalently on their surface (denoted targeted hyaluronan liposomes, or tHA-LIP), can intrinsically provide all requirements for effective drug targeting to tumors. This hypothesis was based on the following elements: 1) many tumors overexpress hyaluronan receptors and/or are rich in extracellular matrix [25−35]; and 2) hyaluronan bound covalently to the liposomal surface [7,8,16, 20−24] may act in two roles (although a single agent): 1) providing the hydrophilic coat for promotion of long circulation; and, as the agent, 2) providing high affinity binding to, and retention at, tumor-localized recognition sites. We have recently reported experimental support for this hypothesis, for tHA-LIP loaded with mitomycin C (MMC), for the treatment of tumor-bearing syngeneic mice [16].

Here we report further testing of the working hypothesis, focusing on HA-LIP loaded with doxorubicin (DXR). The wide use of DXR in the clinic, together with its well-known problems (adverse effects and risks of toxicity), prompted extensive efforts in developing DXR carrier formulations to ameliorate those problems [1−4,17,36]. These efforts include nanosized spheres and nanosized liposomes [1−4,17,36−38]. Two DXR-encapsulating liposomes are approved for human therapy: Doxil/Caelyx and Myocet [1−4,17,36]. Both Doxil and Myocet alter (each product differently) DXR's pharmacokinetics and biodistribution, leading to (product-specific) decreases in DXR-associated toxicities, including its dose-limiting cardiomyopathy and myelosuppression [1−4,17,36].

The present report includes studies in both syngeneic and nude mice. In the syngeneic mice, we studied pharmacokinetics, biodistribution, and therapeutic responses for BALB/c−bearing C-26 solid tumors; C57BL/6−bearing B16F10.9 lung metastasis, and BDF_1-bearing P388/ADR peritoneal ascites. In the nude mice, we studied therapeutic response in a human xenograft model of PANC-1. Performance of our novel formulation was compared with free DXR, DXR encapsulated in regular nontargeted liposomes (nt-LIP), and Doxil, with the latter representing existing DXR carrier formulations, which are closest (in being liposomal and having a hydrophilic coat) to the hyaluronan nanoliposomes.

Materials

Chemicals

High-purity soybean phosphatidylcholine (PC) (Phospholipon 90G) was a kind gift of Nattermann Phospholipid GmbH (Cologne, Germany). All other high-purity lipids, ethyl-dimethyl-aminopropyl-carboiimide (EDC), 3-(4,5-dimethylthiazol-2-yl)-2,5-diphenyl-2H-tetrazolium bromide (MTT), and trypan blue were purchased from Sigma Chemical Co. (St. Louis, MO). DXR was a kind gift from TEVA Pharmaceuticals Industries Ltd. (Natania, Israel). Doxil was purchased from Gamida Cell (Petach-Tikva, Israel). Hyaluronan was a kind gift from Hyal Pharmaceutical Corporation (Toronto, Canada). Cell culture plates and dishes were from Corning Glass Works (New York, NY). Materials for cell cultures (specified under Methods section) were from Biological Industries (Beit Haemek, Israel). Dialysis tubing (molecular weight cutoff of 12,000−14,000) was from Spectrum Medical Industries (Los Angeles, CA). Polycarbonate membranes were from Nucleopore (Pleasanton, CA). All other reagents were of analytical grade.

Instruments

Centrifugation was performed using a Beckman Optima TLX Tabletop ultracentrifuge (Beckman Coulter, Fullerton, CA). Absorbance spectra were measured using a Cary UV−Visible spectrophotometer (Varian Inc., Palo Alto, CA) and a SPECTRA max plate reader PLUS 384 (Molecular Devices Corp., Sunnyvale, CA). Lyophilization was performed with an Alpha 1 to 4 freeze drier (CHRIST, Osterode, Germany). Liposome extrusion was performed with the Lipex extrusion device (Vancouver, Canada). Liposomes were sized by dynamic light scattering using the ALV-NIBS High-Performance Particle Sizer (ALV-GmbH, Langen, Germany). The net surface potential was determined with a Malvern Zetasizer IV (Malvern Instruments, Southborough, MA).

Methods

Preparation and Formulation Properties of Drug-Free and of DXR-Loaded Liposomes (nt-LIP and tHA-LIP)
Preparation of drug-free liposomes

nt-LIP. Multilamellar vesicles (MLVs) were the "raw materials" for the unilamellar vesicles (ULVs) used in this study. MLVs composed of PC:PE:CH at mole ratios of 3:1:1 were prepared by the traditional lipid film method [7−24]. Briefly, the lipids were dissolved in chloroform−methanol (3:1 vol/vol), evaporated to dryness under reduced pressure in a rotary evaporator, and hydrated by the swelling solution that consisted of buffer alone (phosphate-buffered saline, or PBS) at pH 7.2. This was followed by extensive agitation using a vortex device and a 2-hour incubation in a shaker bath at 37°C. The MLVs were extruded through the Lipex device, and operated at room temperature and under nitrogen pressures of 200 to 500 psi. The extrusion was carried out in stages using progressively smaller pore size membranes, with several cycles per pore size, to achieve ULVs in a final size range of <100 nm.

tHA-LIP. Surface modification was performed on the nt-LIP, according to our previously reported procedures [7,8,16,21−24]. Briefly, HA was dissolved in water to a final concentration in the range of 2−5 mg/ml and preactivated by incubation with EDC at pH 4 (controlled by titration with HCl) for 2 hours at 37°C. At the end of this step, the activated HA was added to a suspension of the drug-free nt-LIP, buffered by 0.1 M borate buffer at pH 8.6. Incubation with the liposomes was continued for 24 hours, at 37°C. At the end of the incubation, the liposomes were separated from excess reagents and by-products by centrifugation ($1.3 \times 10^5 g$, 4°C, and 40 minutes) and repeated washings with PBS, reducing the pH back to physiological level. For the present

studies, the final product contained 57 μg HA/μmol lipid. A batch of nt-LIP underwent the same processes, except that water at pH 4 was added instead of the activated HA. The tHA-LIP were lyophilized and kept at −18°C until further use. The lyophilization was performed in 1.0-ml aliquots. Samples were frozen for 2 to 4 hours at −80°C and lyophilized for 48 hours.

Drug encapsulation and properties of final formulations DXR-encapsulating nt-LIP were prepared as described above, except that the swelling solution consisted of DXR dissolved in the PBS. DXR-encapsulating tHA-LIP were prepared by rehydration of the dried powder with an aqueous (pure water) solution of DXR, as previously reported by us for other drugs [16,23,24]. The DXR concentrations in the swelling and rehydration solutions were in the range of 10 ng/ml to 500 μg/ml. Rehydration was performed in the original prelyophilization liposome concentration to retain original buffering and salinity status.

The respective specifications for the tHA-LIP and nt-LIP used in this study, evaluated according to our previously reported procedures [16,23,24] were: diameters of 81 (± 13) and 55 (± 6) nm; zeta potentials of −13.1 (± 3.9) and 0.40 (± 0.01) mV; DXR encapsulation efficiencies of 78 (± 5)% and 54 (± 6)%; and rate constants of 5 (± 0.1) × 10^{-3} and 11 (± 0.2) × 10^{-3} $hour^{-1}$, corresponding to a half-lives of 139 and 63 hours, for the efflux of the encapsulated DXR. Doxil size range was 80 to 90 nm [2,3].

Cell Culture Growth and Maintenance

Monolayers of C-26, B16F10.9, P388/ADR, and PANC-1 cells were grown in 100 × 20 mm dishes (Corning) as previously described [8,16,21,22]. The PANC-1 cells were cultured in Dulbecco's modified Eagle's medium (DMEM). The B16F10.9 cells were cultured in medium containing 10% fetal bovine serum, 0.01 DMEM nonessential amino acids, 1% HEPES buffer (1 M), and 0.01 penicillin−streptomycin. C-26 and P388/Adriamycin (ADR) cells were cultured in RPMI 1640 with 10% fetal calf serum (FCS), penicillin (10,000 U/ml), streptomycin (10 mg/ml), and L-glutamine (200 mM). Suspensions of the P388/ADR cell line were grown in the presence of 250 ng/ml DXR to maintain the multidrug resistance (MDR) phenotype with 3-day washout period before their experimental use. Cells were transferred twice a week and were free of *Mycoplasma* contamination as determined by a *Mycoplasma* ELISA test (Boehringer Mannheim GmbH, Mannheim, Germany) carried out every 3 months. Viability of cultures used in the experiments was >90%, as determined by the trypan blue method.

Mouse Tumor Models, Treatment Protocols, and Measured Parameters

Animals were obtained from the animal breeding center, Tel-Aviv University (Tel Aviv, Israel). Animals were maintained and treated according to National Institutes of Health guidelines. All animal protocols were approved by the Tel-Aviv Institutional Animal Care and Use Committee.

Syngeneic mouse tumor models

Lung metastasis and lung tumor models. The protocols were adapted from Ref. [16]. B16F10.9 cells (5 × 10^5/50 μl PBS) were administered intravenously into 10- to 12-week male C57BL/6 mice. The differences between the metastatic and tumor models depended, as will be shown below, on the day of treatment initiation.

Intraperitoneal ascites model. The protocol was adapted from Ref. [39]. P388/ADR cells were propagated in the peritoneum of 6- to 8-week−old BDF$_1$ female mice by weekly transfer of 0.5 ml of peritoneal fluid containing 5 × 10^5 cells.

Solid tumor model. The protocol was adapted from Ref. [16]. C-26 cells were implanted into the footpad of 8-week−old female BALB/c mice (5 × 10^5 cells/mouse in 30 μl of Hank's buffer).

Human xenograft tumor model

The protocol was adapted from Ref. [40]. Nude CD1-Nu mice (6 weeks old) were housed in barrier facilities on a 12-hour light/dark cycle. Food and water were supplied *ad libitum*. On day 0, 2.5 × 10^6 of PANC-1 cells in 0.1 ml of PBS were implanted subcutaneously just above the right femoral joint.

Treatment Protocols and Measured Parameters

Lung metastatic disease Treatment groups (*n* = 5 per group) included: 1) saline, 2) free DXR, 3) nt-LIP-DXR (i.e., nontargeted DXR-loaded liposomes), 4) Doxil, and 5) tHA-LIP-DXR (i.e., targeted hyaluronan DXR-loaded liposomes). An additional group of untreated tumor-free mice served as control. The dose in each formulation was 10 mg/kg body weight and treatments were on days 1, 5, and 9 from tumor inoculation. Administration was by intravenous injection of 100 μl of the selected formulation to the lateral tail vein, using 26-gauge needles. Two independent experiments were run: one to evaluate lung metastatic burden and the other to evaluate survival. For evaluation of lung metastatic burden, the experiment was terminated 21 days post−tumor injection. The lungs of all animals in the experiment were removed, weighted, and fixed in Bouin's solution. Increase in lung weight was calculated using the following formula [16]: Lung weight increase (%) = 100 × (tumor lung weight − normal lung weight) / normal lung weight. Surface metastases were counted, using a dissecting microscope, by a pathologist blinded to the experimental groups involved. For evaluation of survival, animals were monitored daily, and the experiment was terminated on day 90.

Lung tumor model

Pharmacokinetics. The experiment was performed 10 days after tumor inoculation. Plasma clearance studies were performed with the tumor-bearing and healthy animals, both from the C57BL/6 strain. Administration details and treatment groups (*n* = 10 per group) were as listed above for the lung metastatic model, except omission of the saline group. All formulations were equal in the injected drug dose,

10 mg/kg body weight. Blood samples were collected over a time span of 72 hours postinjection by retrobulbar puncture.

The blood samples were immediately mixed with 250 μl of 0.5 mM EDTA−PBS, followed by a 5-minute centrifugation at 200g. DXR was assayed in both cell and supernatant fractions, as follows: the pelleted cells and the supernatant from the first centrifugation were separated, and the cells were subjected to a wash (including recentrifugation) in the EDTA−PBS solution. The supernatants from both runs were combined and assayed for DXR. DXR was extracted from the cells by incubation with 2.5 ml of acidic isopropanol (81 mM HCl in isopropanol) for 4 hours at 4°C, followed by centrifugation under the same conditions specified above. The supernatants, containing the extracted DXR, were also subjected to assay and found to contain negligible amounts of DXR (< 0.001% of injected dose).

Calculation of area under the curve (AUC) of concentration *versus* time was performed using the WinNonLin 4.0.1 program (Pharsight Corporation, Mountain View, CA) by a NonCompartment model 201 (intravenous bolus administration).

Tissue distribution. The experiment was performed 10 days after tumor implantation and included two groups of C57BL/6 mice. One group was inoculated with B16F10.9 cells to bear lung tumors; the other group was that of healthy mice. Each group was divided into four subgroups (n = 7 per subgroup), receiving a single intravenous dose of a selected formulation on day 10 from tumor inoculation. Treatment groups included: tHA-LIP-DXR, nt-LIP-DXR, Doxil, and free DXR. Drug dose in all cases was 10 mg/kg body weight, and details of administration are as listed above for pharmacokinetics. Six hours postinjection, the mice were anesthesized and sacrificed. Liver, spleen, kidneys, and lungs were removed immediately after perfusion with saline and each organ was examined by a pathologist blinded to the experimental groups involved. Each organ was then homogenized; DXR was extracted from it as described above for pharmacokinetics, and assayed.

Intraperitoneal ascites model. Administration details and treatment groups (n = 7 per group) were as detailed above for the lung metastatic disease model. The dose in each formulation was 3 mg/kg body weight and treatments were given on days 1, 5, and 9 from tumor inoculation. Survival of all animals was monitored continuously.

Solid tumor model. Animal groups (n = 5 per group), treatment formulations, drug doses, and method of administration were as described above for the lung metastatic disease model. Treatments were initiated after the development of an easily palpable tumor (5 days), and given on days 5, 12, 19, and 26 post−tumor inoculation. Tumor size was measured, using an electronic caliper, every other day for the next 30 days. Tumor volume was calculated by using the following formula [16]: Tumor volume = 1/2(width)^2 × length. Animal survival was monitored continuously, and the experiment was terminated on day 110. Pharmacokinetics was studied as described above for the lung tumor model.

PANC-1 xenografts in nude mice Treatments were initiated when tumor volumes reached 75 mm^3 (day 0). The mice were randomly separated into four groups (n = 10 per group): 1) saline, 2) free DXR, 3) Doxil, and 4) tHA-LIP-DXR. Administration route and protocol were as described above for the lung metastatic disease mode. DXR dose in each formulation was 10 mg/kg body weight and treatments were on days 0, 7, and 14. Tumor volume was calculated as: (length - × width) × [(length + width) / 2] [40].

Quantitative Determinations

DXR was assayed by its florescence, using 470 nm as the excitation wavelength and 582 nm as the emission wavelength. The quantity of viable cells was determined by: 1) the MTT test, recording the absorbencies in a plate reader at two wavelengths 550 and 650 nm [16]; 2) total cell protein by the Bradford assay; and 3) the trypan blue method.

Statistics

Statistical significance was evaluated by using two-tailed Student's t test.

Results

Pharmacokinetics of Free and of Liposomal DXR in Healthy and Tumor-Bearing Mice

Free DXR was rapidly eliminated from the circulation in both healthy and tumor-bearing mice (Figure 1, $A-C$). Formulating DXR in liposomes extended its retention in circulation, modestly by nt-LIP and substantially by Doxil and tHA-LIP (Figure 1, $A-C$). The AUC ratios for tHA-LIP/ free DXR, tHA-LIP/nt-LIP, and tHA-LIP/Doxil were: a) 147, 19, and 4 in the healthy C57BL/6 mice; b) 53, 5, and 1.3 in the B16F10.9−bearing C57BL/6 mice; and c) 110 , 8.6, and 2.6 in the C-26−bearing BALB/c mice.

Interestingly, for three of the DXR formulations—free DXR, nt-LIP-DXR, and Doxil—the absolute AUC numbers (in hr μg/ml) did not change dramatically between the tumor-bearing (Figure 1A) and the healthy (Figure 1B) C57BL/6 mice. In contrast, the absolute AUC value for the test formulation, tHA-LIP-DXR, dropped from 1280 hr μg/ml in the healthy mice to 408 hr μg/ml in the tumor-bearing mice. The acceleration in clearance, from the healthy to the tumor-bearing animals, could result from an increase in RES clearance or in drug accumulation within the tumor. For therapy, the former would be a negative outcome, and the latter would be a positive outcome. The biodistribution studies, reported in Biodistribution of Free and of Liposomal DXR in Healthy and Tumor-Bearing C57BL/6 Mice section, shed light on this matter.

Biodistribution of Free and of Liposomal DXR in Healthy and Tumor-Bearing C57BL/6 Mice

Pathology examination found tumors in the lungs of the animals injected with B16F10.9 cells, whereas their spleens, kidneys, and livers were found to be tumor-free. The sequence of DXR uptake in the tumor-free organs was: free drug > nt-LIP > Doxil > tHA-LIP (Figure 2A). In liver and
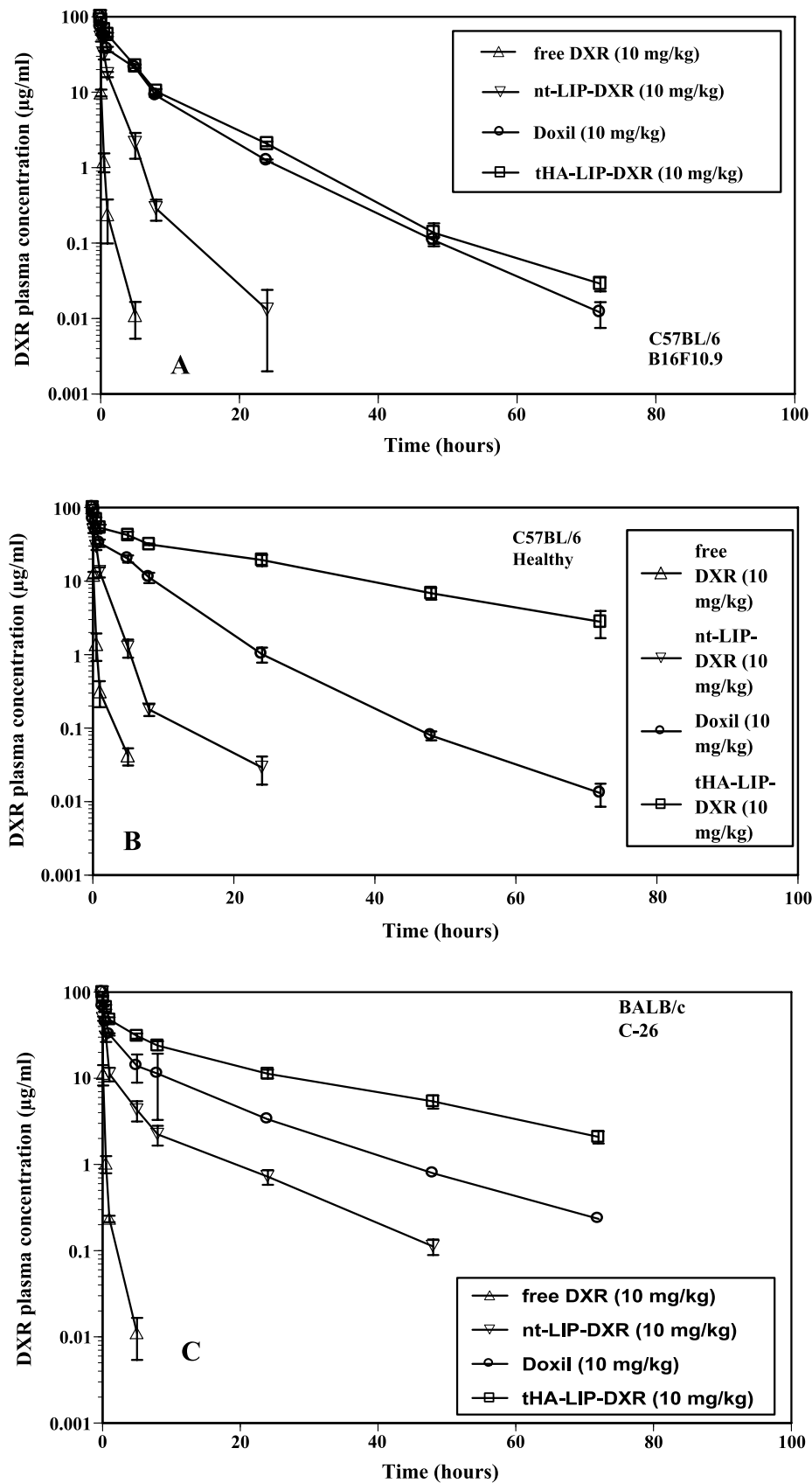
Figure 1. *DXR plasma concentration (μg/ml) as a function of time from dosing. (A) C57BL/6 mice inoculated (by intravenous injection) with B16F10.9 cells. (B) Healthy C57BL/6 mice. (C) BALB/c mice inoculated with C-26 cells (injected into the right-hind footpad). A single dose of the selected formulation was injected to the tail vein. DXR formulations and doses are specified within the figure. The points are experimental, each an average from all animals in the group (n = 10 per group). The error bars represent the SD. The solid curves are nontheoretical, drawn to emphasize the trends in the data.*

spleen, encapsulation in the tHA-LIP lowered DXR uptake significantly, compared with free drug ($P < .01$), DXR in the nt-LIP ($P = .039$ and $P = .042$, respectively), and Doxil ($P = .05$ for the liver and no statistical significance compared with the spleen). This sequence was reversed (tHA-LIP > Doxil > nt-LIP > free drug) for DXR uptake into the tumor (Figure 2B). Mediated by the tHA-LIP, drug uptake into tumor was 3.5-, 6.7-, and 30-fold higher compared with Doxil ($P = .011$), nt-LIP ($P < .001$), and free drug ($P < .001$), respectively. This sequence, and especially the enhanced DXR tumor accumulation mediated by tHA-LIP, was tumor-specific rather than organ-specific. This is seen from the findings for healthy animals (Figure 2C), where drug uptake into the lungs was negligible irrespective of whether the drug was free or formulated in the various liposome systems. The vehicles themselves (i.e., drug-free nt-LIP and tHA-LIP) were inactive in this and all other mouse tumor models [16].

Therapeutic Responses of Mice Bearing B16F10.9-Originating Lung Metastatic Disease

The metastatic burden, measured by two independent parameters—increase in lung weight and number of lung metastasis—was highest for the saline group (Figure 3A). The burden remained high on treatments with free drug or drug-encapsulating nt-LIP and the situation was modestly better on treatment with Doxil (Figure 3A). Treatment with the DXR-loaded tHA-LIP induced, in contrast, a significant reduction in lung metastatic burden ($P < .001$ compared with free drug): increase in lung weight was only 29% over normal lungs (normal lung weight at day 21 was 0.21 ± 0.03 g), with a concomitant small number (<10) of lung metastasis (Figure 3A). These encouraging results were mirrored by the survival data (Figure 3B). Treatment with DXR-loaded tHA-LIP generated a substantial and significant increase in survival ($P < .0007$, $P < .001$, and $P < .01$) compared with free drug , DXR-loaded nt-LIP, and Doxil, respectively.
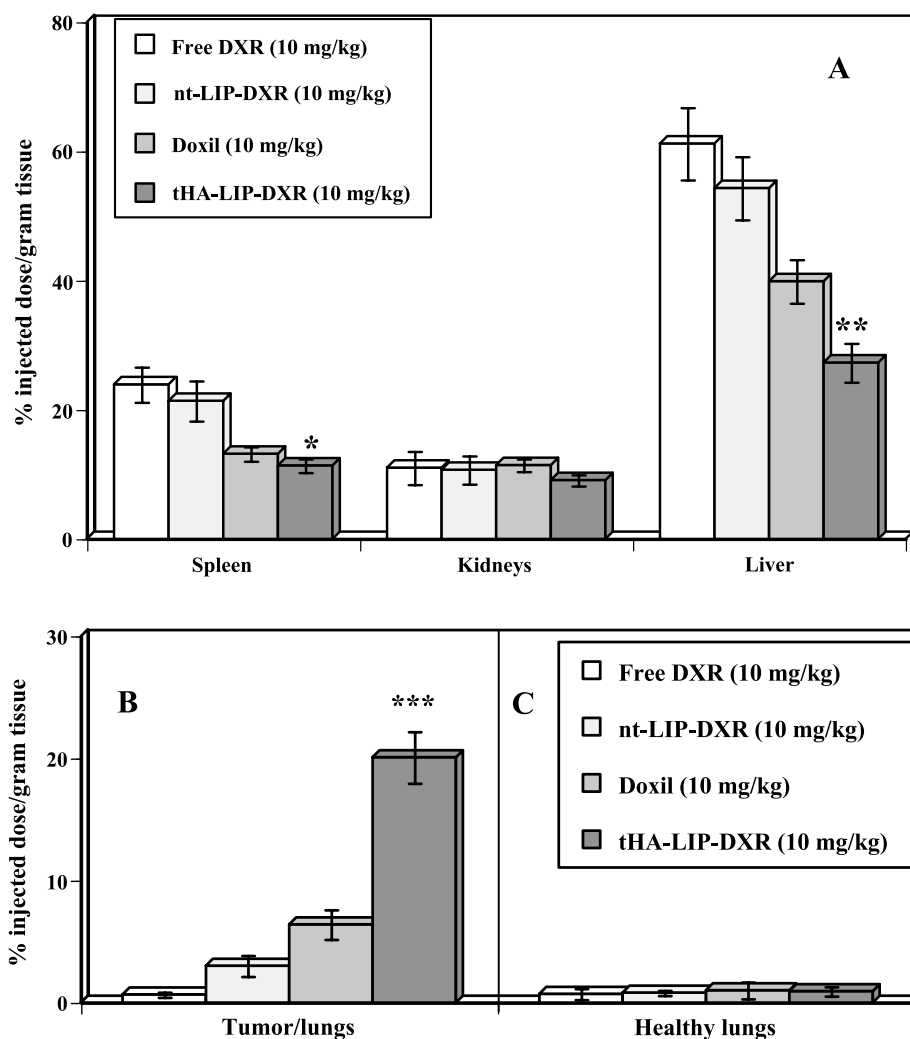

Figure 2. *Drug biodistribution (percentage of injected dose per gram of tissue) in healthy and B16F10.9 tumor-bearing C57BL/6 mice (n = 7 per group). (A) Biodistribution in selected non–tumor-bearing organs of B16F10.9-inoculated animals. (B) Biodistribution in the tumor-bearing lungs of B16F10.9-inoculated animals. (C) Biodistribution in the lungs of healthy animals. Inoculation of tumor cells and drug administration were as listed under Figure 1. DXR formulations and doses are specified within the figure. Each bar is an average from all animals in the group and the error bars represent the SD. Statistical significance evaluations represented on the figure by asterisks are comparisons of selected formulation to free DXR (***P < .001, **P < .01, *P < .05).*
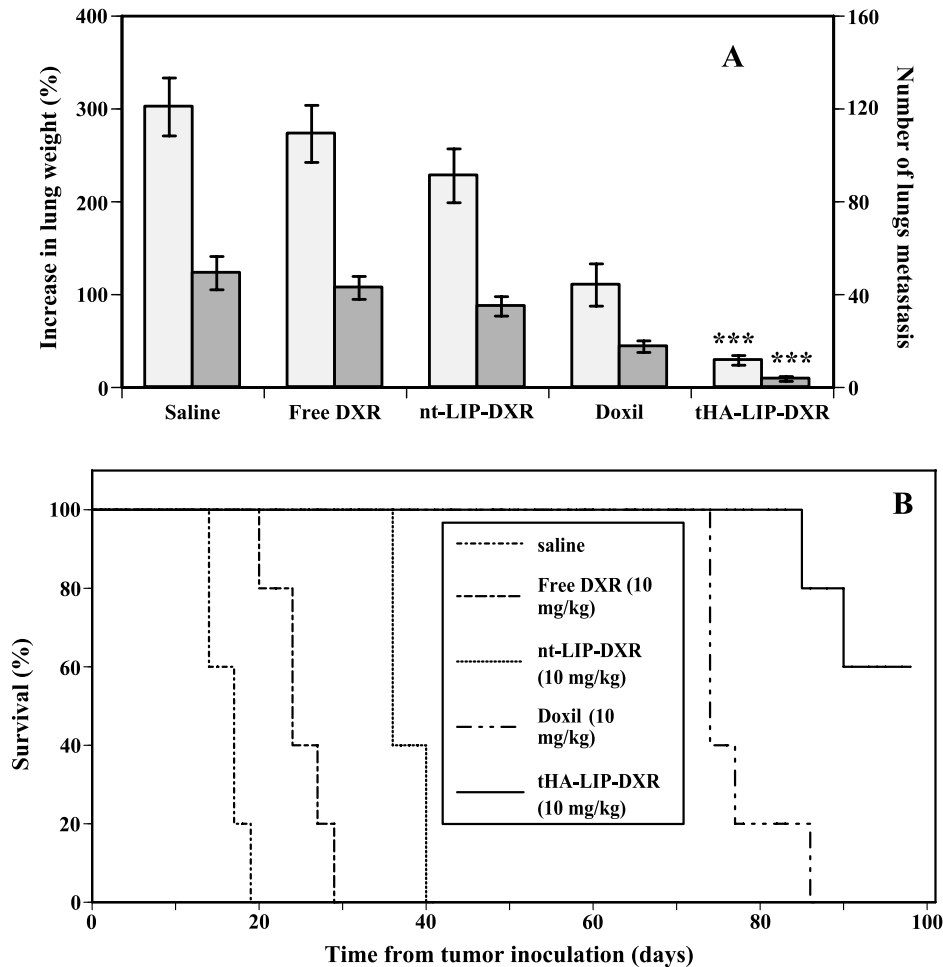
Figure 3. *Therapeutic responses of mice bearing B16F10.9-originating lung metastatic disease. DXR formulations and doses are specified within the figure. Treatments were on days 1, 5, and 9 by injection of the selected formulation to the tail vein. (A) Lung metastatic burden. Light-shaded bars are the data for the increase in lung weight; dark-shaded bars are the data for the number of lung metastasis. Each bar is an average of all animals in the group (n = 5) and the SD is represented by the error bars. ***Indicates P < .001 compared with free drug. (B) Survival (n = 5). Each line connects the symbols representing the daily survival state of the group; the symbols themselves were omitted to avoid a cluttered figure.*

Survival of BDF$_1$ Mice Bearing Drug-Resistant (P388/ADR) Intraperitoneal Ascites Tumors

Survival of animals implanted with these MDR cells was unaffected by treatment with DXR alone, and showed poor response to treatment with Doxil or DXR-loaded nt-LIP (Figure 4). In contrast, treatment with the DXR-loaded tHA-LIP generated a considerable increase in the survival rate—five-fold to six-fold increases in life span compared with the treatment with free DXR, Doxil, and DXR-loaded nt-LIP (Figure 4).

Therapeutic Responses of BALB/c Mice Bearing C-26 Solid Tumors

Tumor volumes increased rapidly and exponentially when animals were treated with saline alone, free DXR, or DXR-loaded nt-LIP (Figure 5A), with little difference among these three treatment groups. Tumor was detectable in all these groups at day 7 postinoculation. Treatment with Doxil and DXR-loaded tHA-LIP slowed the tumor growth rate signifi-

cantly. The tumors in the animals receiving the DXR-loaded tHA-LIP were smallest among all five groups, and were first detected on day 16—more than two-fold delay compared
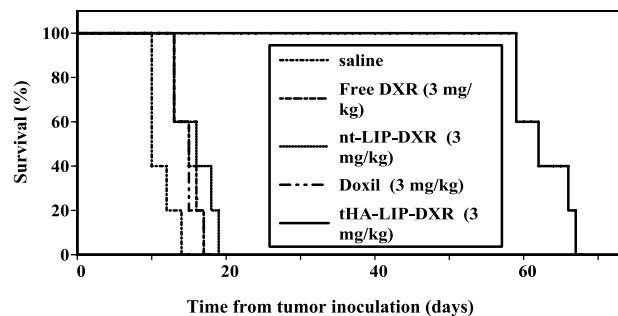

Figure 4. *Survival of BDF$_1$ female mice bearing intraperitoneal ascites tumor generated through intraperitoneal implants of P388/ADR cells. DXR formulations and doses are specified within the figure. Each line connects the symbols representing the daily survival state of the group (n = 7). The symbols themselves were omitted to avoid a cluttered figure.*

with all other groups (Figure 5*A*). These results were also mirrored by the survival data (Figure 5*B*). Treatment with DXR-loaded tHA-LIP was distinctly different that the other four groups, resulting in highly prolonged survival ($P < .0007$ and $P < .001$) compared with free drug, drug-loaded nt-LIP, and Doxil, respectively.

Therapeutic Responses in Nude Mice Bearing PANC-1 Xenografts

At the day of treatment initiation, tumor volumes in all treatment groups were 70 to 75 mm³. Tumors in the animals treated with saline or free DXR continued to grow rapidly with no significant distinction between the two groups (Figure 6). During the first 12 to 14 days of treatment, response of

the animals treated with Doxil was not much different than in the case of saline and free DXR. It took the full treatment course (three doses) for the impact of Doxil to emerge: tumor growth seemed arrested between days 14 and 20, and started growing again at a slow pace thereafter, reaching, at day 32, tumor volumes eight-fold higher than at initiation of treatment (Figure 6).

The response of the animals treated with DXR-loaded tHA-LIP was strikingly different (Figure 6): tumor growth was arrested on the first treatment and, thereafter, with time and completion of full treatment course, there was significant tumor shrinkage. Tumor volumes at day 32 were six-fold smaller that at initiation of treatment. Moreover, 4 if 10 mice in this group were tumor-free on day 32.
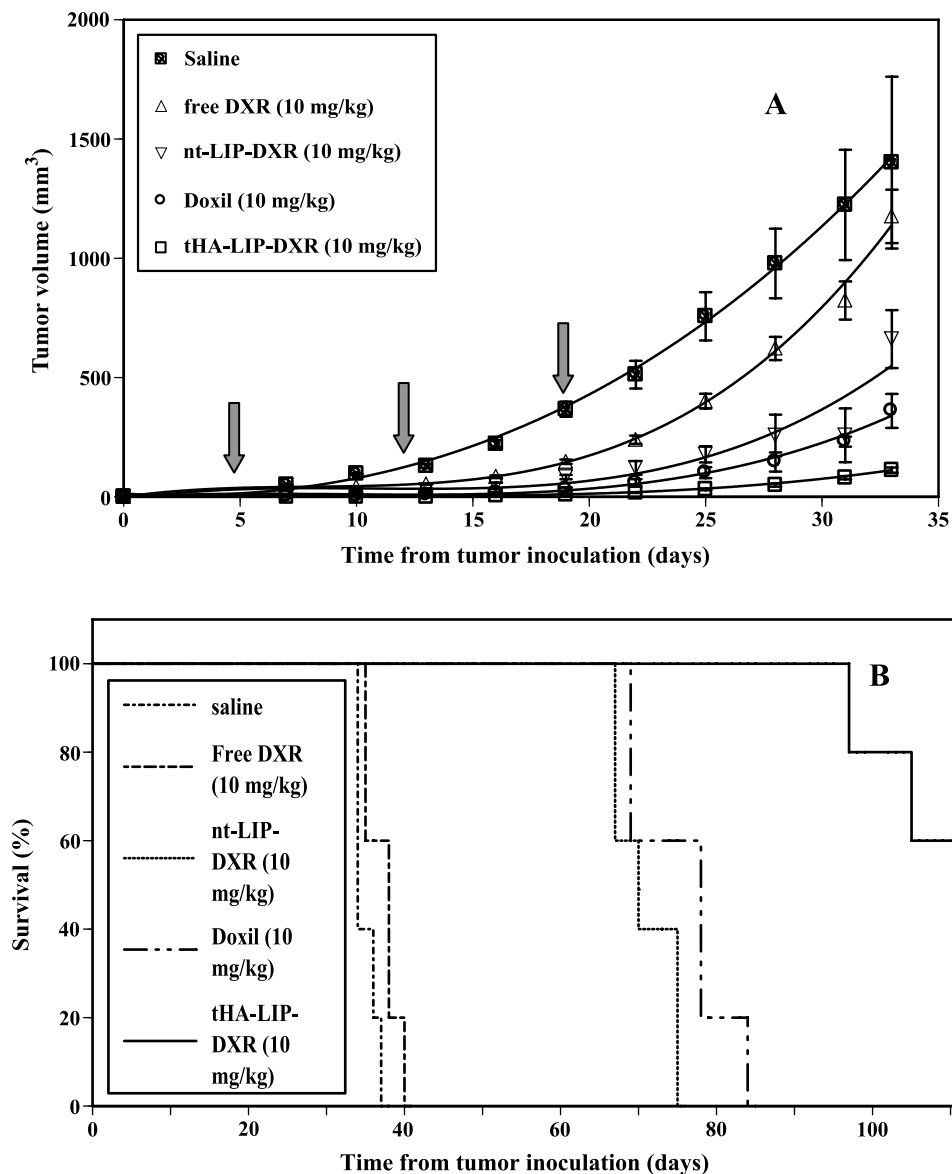

Figure 5. *Therapeutic responses of BALB/c mice inoculated with C-26 cells injected to the right-hind footpad. Treatments were on days 5, 12, and 19 (indicated by the arrows in the figure), by injection of the selected formulation to the tail vein. DXR formulations and doses are specified within the figure. (A) Increase in tumor volume. The points are the experimental data, each an average of all animals in the group (n = 5), and the SEM are represented by the error bars. The solid curves are nontheoretical, drawn to emphasize the trends in the data. (B) Survival. Each line connects the symbols representing the daily survival state of the group (n = 5). The symbols themselves were omitted to avoid a cluttered figure.*
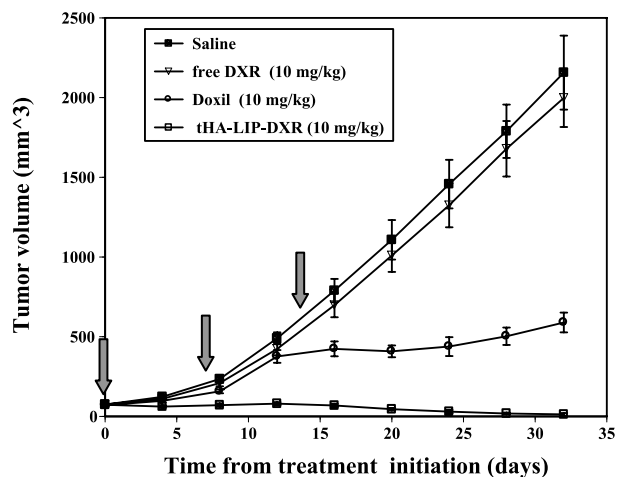
Figure 6. *Increase in tumor volume of nude CD1-Nu mice inoculated with PANC-1 cells implanted subcutaneously just above the right femoral joint. Treatments were initiated when tumor volumes reached 75 mm^3 (day 0) and were given on days 0, 7, and 14 (as indicated by the arrows in the figure), by injection of the selected formulation to the tail vein. DXR formulations and doses are specified within the figure. The points are the experimental data, each an average of all animals in the group (n = 10), and the SEM are represented by the error bars. The solid curves are nontheoretical, drawn to emphasize the trends in the data.*

Discussion

The varied levels of response that different tumors have for the same anticancer drug, the impact of adverse effects, and the frequent problem of drug resistance often undermine the clinical outcomes of tumor treatment. Among the major approaches to counter this dire situation are the continuous efforts to increase the arsenal of existing anticancer agents, by novel drugs and by new formulations of veteran drugs. A case in point is DXR, the anticancer drug at the center of the present study, where the two approved liposomal formulations generate different clinical responses and are currently approved for different indications [17]. To merit consideration for the clinical arsenal, a veteran drug in a novel carrier formulation should provide active drug targeting to the tumor. Such targeting should, furthermore, generate significant improvement in therapeutic responses, in more than one tumor model. In the study reported here, we addressed all of these requirements, at their preclinical stage. The rationale for selecting (of the two approved DXR liposome formulations) Doxil as a representative of approved DXR carrier formulations was discussed in the Introduction. We would like to note that, where it was possible to compare, performance of Doxil at our hands was similar to previous reports in the field [41].

Determining DXR pharmacokinetics and biodistribution, it became clear that although free DXR is removed fast from the circulation, removal was delayed by enclosure of the drug in particulate carriers (Figure 1). The delay was shortest for the nt-LIP, and quite significant for Doxil and tHA-LIP, with circulation of the latter either similar to, or longer than, Doxil (Figure 1, A–C). Both Doxil and tHA-LIP probably benefited from their combination of small sizes and hydrophilic coats. The phenomenon itself was independent of mouse strain,

mouse health status, and tumor model, but differed quantitatively among the systems tested. The similarity in the ability of tHA-LIP to induce long-term circulation, for two different (encapsulated) drugs [16], also implies that this property is drug-independent. This confirms the working hypothesis that the HA positioned at the liposomal surface provides the hydroxyl residues necessary to endow particulate carriers with a hydrophilic coat for promotion of long-term retention in circulation.

DXR uptake into the tumor-free spleen and kidneys was not very sensitive to the nature of drug formulation, whereas drug uptake into the tumor-free liver was significantly reduced when the drug was delivered through tHA-LIP or Doxil (Figure 2A). In contrast, drug accumulation in tumor-bearing (Figure 2B), but not in healthy (Figure 2C), lungs was significantly affected by carrier mediation. When delivered through tHA-LIP, DXR accumulation in the tumor was 30-fold higher than when the drug was administered in free form, 6.7-fold higher than when delivered through nt-LIP, and 3-fold when delivered with Doxil (Figure 2B). That the tumor, rather than the anatomic location, made the difference can be appreciated from selectivity, defined as the ratio of drug uptake into the lungs of tumor-bearing mice, compared with the same organ in healthy (tumor-free) animals. We obtained a selectivity of 20 (Figure 2, B and C), which is higher than reported for DXR-encapsulating sterically stabilized regular and immunoliposomes [2–4,9–11,41].

Next was the question of whether the achievement of drug targeting has a positive impact on therapeutics. *In vitro* studies showed that encapsulation of DXR in tHA-LIP generated a 10- to 100-fold reduction in the drug's IC_{50} values compared with free DXR, but only in cell lines that over-express HA receptors (data not shown). The cumulative *in vivo* data following tumor size, metastatic burden, and survival (Figures 3–6) are clear indications of the positive impact targeting had on therapeutic responses. In C57BL/6 mice bearing lung metastatic disease, treatments with free DXR or DXR-encapsulating nt-LIP were not much different from one another or from no treatment (saline) in reducing lung metastatic burden (Figure 3A) and in increasing survival (Figure 3B). Significant improvements, in both metastatic burden and survival, were obtained with Doxil and more so with the DXR-loaded tHA-LIP (Figure 3, A and B). The impact of formulation in the tHA-LIP is even more striking for the BDF$_1$ mice bearing an acquired MDR ascites tumor. Animals treated with saline, free DXR, DXR-encapsulating nt-LIP, and Doxil showed poor survival that was not much different among these formulations (Figure 4). Only treatment with DXR-encapsulating tHA-LIP generated a substantial difference, tripling the life span (Figure 4). Treatment of BALB/c mice bearing solid tumors, with free DXR, was not much different than saline—fast exponential tumor growth and poor survival (Figure 5, A and B). Carrier mediation slowed down tumor progression and increased survival in all three liposomal formulations, tHA-LIP > Doxil > nt-LIP (Figure 5, A and B). The strength of the novel targeted formulation was seen especially in the survival data (Figure 5B).

Benefits of the DXR-loaded tHA-LIP formulation were not restricted to mouse-originating tumors, as shown for the solid tumors generated in nude mice by xenografts of human pancreatic adenocarcinoma (PANC-1). The attempts to cause tumor shrinkage failed when treatment was with saline or free drug, with the tumors continuing their fast growth pattern (Figure 6). It took the three Doxil doses for temporary arrest of tumor progression, followed by slow growth (Figure 6). The attempts were successful only when treatment was by novel targeted formulation (DXR-loaded tHA-LIP), continuous tumor shrinkage, and, in some cases (4 of 10), complete regression (Figure 6).

To summarize, DXR-encapsulating tHA-LIP generated significant improvements in clinical outcomes in four different mouse species (C57BL/6, BALB/C, BDF1, and athymic nude mice), in tumors generated in different organs, and in tumors originating from different cell lines (B16F10.9, C-26, P388/ADR, and PANC-1)—the common factor among them being tumors that overexpress hyaluronan receptors [16,32,42]. In this respect, the hyaluronan itself may have contributed to the positive outcome. It has been suggested that hyaluronan receptors in tumor cells are involved in tumor progression, and that blocking these receptors can slow down the process [29–31,33]. It may be that when the tHA-LIP bind to the hyaluronan receptors at the tumor, they perform two roles: act as a depot of the chemotherapeutic drug and, at the same time, slow down tumor progression by blocking the receptors.

In conclusion, we suggest that on the basis of the present results, DXR-loaded tHA-LIP deserve consideration as candidate for the anticancer drug arsenal and merit further pursuit in the many types of tumors that overexpress hyaluronan receptors. This formulation is distinct in having cryoprotection [24], long circulation, and high affinity to the target, all provided by the same single (naturally occurring) agent—hyaluronan anchored to the liposomal surface.

References

[1] Allen TM (2002). Ligand-targeted therapeutics in anticancer therapy. *Nat Rev Cancer* **2,** 750–763.

[2] Gabizon AA (2002). Liposomal drug carrier systems in cancer chemotherapy: current status and future prospects. *J Drug Target* **10,** 535–538.

[3] Gabizon A, Shmeeda H, and Barenholz Y (2003). Pharmacokinetics of pegylated liposomal Doxorubicin: review of animal and human studies. *Clin Pharmacokinet* **42,** 419–436.

[4] Sapra P and Allen TM (2003). Ligand-targeted liposomal anticancer drugs. *Prog Lipid Res* **42,** 439–462.

[5] Kim JA (2003). Targeted therapies for the treatment of cancer. *Am J Surg* **186,** 264–268.

[6] Goldman JM and Melo JV (2003). Chronic myeloid leukemia—advances in biology and new approaches to treatment. *N Engl J Med* **349,** 1451–1464.

[7] Margalit R (1995). Liposome-mediated drug targeting in topical and regional therapies. *Crit Rev Ther Drug Carr Syst* **12,** 233–261.

[8] Margalit R (1998). Bioadhesive liposomes in topical treatment of wounds. In Berenstein, CH (Ed.), Microparticulates—Preparation, Characterization and Application in Medicine, pp. 425–461 Marcel Dekker, Inc., New York.

[9] Gabizon AA (2001). Pegylated liposomal doxorubicin: metamorphosis of an old drug into a new form of chemotherapy. *Cancer Invest* **19,** 424–436.

[10] Moghimi SM, Hunter AC, and Murray JC (2001). Long-circulating and target-specific nanoparticles: theory to practice. *Pharmacol Rev* **53,** 283–318.

[11] Forssen EA, Coulter DM, and Proffit RC (1992). Selective localization of daunorubicin small unilamellar vesicles in solid tumors. *Cancer Res* **52,** 3255–3261.

[12] Allen TM (1994). Long-circulating (sterically stabilized) liposomes for targeted drug delivery. *Trends Pharmacol Sci* **15,** 215–220.

[13] Oku N and Namba Y (1994). Long-circulating liposomes. *Crit Rev Ther Drug Carr Syst* **11,** 231–270.

[14] Tardi P, Choice E, Masin D, Redelmeier T, Bally M, and Madden TD (2000). Liposomal encapsulation of topotecan enhances anticancer efficacy in murine and human xenograft models. *Cancer Res* **60,** 3389–3393.

[15] Papahadjopoulos D, Allen TM, Gabizon A, Mayhew E, Matthay K, Huang SK, Lee KD, Woodle MC, Lasic DD, and Redemann C (1991). Sterically stabilized liposomes: improvements in pharmacokinetics and antitumor therapeutic efficacy. *Proc Natl Acad Sci USA* **88,** 11460–11464.

[16] Peer D and Margalit R (2004). Loading mitomycin C inside long-circulating hyaluronan targeted nano-liposomes increases its antitumor activity in three mice tumor models. *Int J Cancer* **108,** 780–789.

[17] Waterhouse DN, Tardi PG, Mayer LD, and Bally MB (2001). A comparison of liposomal formulations of doxorubicin with drug administered in free form: changing toxicity profiles. *Drug Saf* **24,** 903–920.

[18] Tseng YL, Hong RL, Tao MH, and Chang FH (1999). Sterically stabilized anti–idiotype immunoliposomes improve the therapeutic efficacy of doxorubicin in a murine B-cell lymphoma mode. *Int J Cancer* **80,** 723–730.

[19] Koning GA, Morselt HW, Gorter A, Allen TM, Zalipsky S, Kamps JA, and Scherphof GL (2001). Pharmacokinetics of differently designed immunoliposome formulations in rats with or without hepatic colon cancer metastases. *Pharm Res* **18,** 1291–1298.

[20] Yerushalmi N and Margalit R (1994). Bioadhesive, collagen-modified liposomes: molecular and cellular level studies on the kinetics of drug release and on binding to cell monolayers. *Biochim Biophys Acta* **1189,** 13–20.

[21] Yerushalmi N, Arad A, and Margalit R (1994). Molecular and cellular studies of hyaluronic acid–modified liposomes as bioadhesive carriers for topical drug delivery in wound healing. *Arch Biochem Biophys* **313,** 267–273.

[22] Yerushalmi N and Margalit R (1998). Hyaluronic acid–modified bioadhesive liposomes as local drug depots: effects of cellular and fluid dynamics on liposome retention at target sites. *Arch Biochem Biophys* **349,** 21–26.

[23] Peer D and Margalit R (2000). Physicochemical evaluation of a stability-driven approach to drug entrapment in regular and in surface-modified liposomes. *Arch Biochem Biophys* **383,** 185–190.

[24] Peer D, Florentin A, and Margalit R (2003). Hyaluronan is a key component of cryoprotection and formulation of targeted unilamellar liposomes. *Biochim Biophys Acta* **1612,** 76–82.

[25] Zöller M (1995). CD44: physiological expression of distinct isoforms as evidence for organ-specific metastasis formation. *J Mol Med* **73,** 425–438.

[26] Smadja-Joff F, Legras S, Girard N, Li Y, Delpech B, Bloget F, Morimoto K, Le Bousse-Kerdile C, Clay D, Jasmin C, and Levesque JP (1996). CD44 and hyaluronan binding by human myeloid cells. *Leuk Lymphoma* **21,** 407–420.

[27] Rudzki Z and Jothy S (1997). CD44 and the adhesion of neoplastic cells. *Mol Pathol* **50,** 57–71.

[28] Sneath RJ and Mangham DC (1998). The normal structure and function of CD44 and its role in neoplasia. *Mol Pathol* **51,** 191–200.

[29] Tran TA, Kallakury BV, Sheehan CE, and Ross JS (1997). Expression of CD44 standard form and variant isoforms in non-small cell lung carcinomas. *Hum Pathol* **28,** 809–814.

[30] Gallatin M, St Joh TP, Siegelman M, Reichert R, Butcher EC, and Weissman IL (1986). Lymphocyte homing receptors. *Cell* **44,** 673–680.

[31] Li H, Guo L, Li JW, Liu N, Qi R, and Liu J (2000). Expression of Hyaluronan receptors CD44 and RHAMM in stomach cancers: relevance with tumor progression. *Int J Oncol* **17,** 927–932.

[32] Abetamann V, Kern HF, and Elsasser HP (1996). Differential expression of the hyaluronan receptors CD44 and RHAMM in human pancreatic cancer cells. *Clin Cancer Res* **2,** 1607–1618.

[33] Bartolazzi A, Peach R, Aruffo A, and Stamenkovic I (1994). Interaction between CD44, and hyaluronate is directly implicated in the regulation of tumor development. *J Exp Med* **180,** 53–66.

[34] Chiu RK, Carpenito C, Dougherty ST, Hayes GM, and Dougherty GJ (1999). Identification and characterization of CD44RC, a novel alternatively spliced soluble CD44 isoform that can potentiate the hyaluronan binding activity of cell surface CD44. *Neoplasia* **1,** 446–452.

[35] Birch M, Mitchell S, and Hart IR (1991). Isolation and characterization of human melanoma cell variants expressing high and low levels of CD44. *Cancer Res* **51,** 6660–6667.

[36] Harris L, Batist G, Belt R, Rovira D, Navari R, Azarnia N, Welles L, and Winer E (2002). Liposome-encapsulated doxorubicin compared with conventional doxorubicin in a randomized multicenter trial as first-line therapy of metastatic breast carcinoma. *Cancer* **94,** 25–36.

[37] Mitra S, Gaur U, Ghosh PC, and Maitra AN (2001). Tumour targeted delivery of encapsulated dextran–doxorubicin conjugate using chitosan nanoparticles as carrier. *J Control Release* **74,** 317–323.

[38] Yoo HS, Lee KH, Oh JE, and Park TG (2000). *In vitro* and *in vivo* antitumor activities of nanoparticles based on doxorubicin–PLGA conjugates. *J Control Release* **68,** 419–431.

[39] Newman MJ, Rodarte JC, Benbatoul KD, Romano SJ, Zhang C, Krane S, Moran EJ, Uyeda RT, Dixon R, Guns ES, and Mayer LD (2000). Discovery and characterization of OC144-093, a novel inhibitor of P-glycoprotein–mediated multidrug resistance. *Cancer Res* **60,** 2964–2972.

[40] Gana-Weisz M, Halaschek-Wiener J, Jansen B, Elad G, Haklai R, and Kloog Y (2002). The Ras inhibitor *S-trans*, *trans*-farnesylthiosalicylic acid chemosensitizes human tumor cells without causing resistance. *Clin Cancer Res* **8,** 555–565.

[41] Gabizon A, Tzemach D, Mak L, Bronstein M, and Horowitz AT (2002). Dose dependency of pharmacokinetics and therapeutic efficacy of pegylated liposomal doxorubicin (DOXIL) in murine models. *J Drug Target* **10,** 539–548.

[42] Droll A, Dougherty ST, Chiu RK, Dirks JF, McBride WH, Cooper DL, and Dougherty GJ (1995). Adhesive interactions between alternatively spliced CD44 isoforms. *J Biol Chem* **270,** 11567–11573.